Transmission of Plasticity Through Grain Boundaries in a Metastable Austenitic Stainless Steel

Antonio Mateo [1],* [ID], Ina Sapezanskaia [1,2], Joan Josep Roa [1], Gemma Fargas [1] and Abdelkrim Redjaïmia [2] [ID]

[1] CIEFMA (Center for Research in Structural Integrity, Reliability and Micromechanics of Materials), Departament de Ciència dels Materials i Enginyeria Metal·lúrgica, Universitat Politècnica de Catalunya, 08034 Barcelona, Spain; mailforinna@gmx.de (I.S.); joan.josep.roa@upc.edu (J.J.R.); gemma.fargas@upc.edu (G.F.)

[2] Institut Jean Lamour, UMR CNRS (Unité Mixte de Recherche du Centre National de Recherche Scientifique) 7198, Université de Lorraine, 54000 Nancy, France; Abdelkrim.Redjaimia@univ-lorraine.fr

* Correspondence: antonio.manuel.mateo@upc.edu; Tel.: +34-93401-1089

Abstract: Austenitic metastable stainless steels have outstanding mechanical properties. Their mechanical behavior comes from the combination of different deformation mechanisms, including phase transformation. The present work aims to investigate the main deformation mechanisms through the grain boundary under monotonic and cyclic tests at the micro- and sub-micrometric length scales by using the nanoindentation technique. Within this context, this topic is relevant as damage evolution at grain boundaries is controlled by slip transfer, and the slip band-grain boundary intersections are preferred crack nucleation sites. Furthermore, in the case of metastable stainless steels, the interaction between martensitic phase and grain boundaries may have important consequences.

Keywords: martensitic transformation; plastic deformation mechanisms; monotonic and cyclic nanoindentation tests; grain boundary; Focused Ion Beam (FIB)

1. Introduction

Some austenitic stainless steel grades, particularly those with low Stacking Fault Energy (SFE), can undergo deformation-induced martensitic transformation [1]. For this reason, they are designated as metastable steels. Studying the deformation behavior of metastable stainless steels is appealing because on the one hand several deformation mechanisms can be simultaneously activated, while on the other hand there is great interest in those steels for automotive applications [2]. Consequently, a comprehensive understanding of their local mechanical properties is essential for improving their performance and properly tailoring the manufacturing of industrial components fabricated with them.

When straining metastable stainless steels, austenite grains exhibit dislocation slip and twinning, but their main characteristic is the susceptibility to the Transformation-Induced Plasticity (TRIP) effect, whereby austenite to martensite transformation is triggered mechanically [3,4]. Conventional studies at the macroscopic scale are not appropriate to completely understand all of the deformation mechanisms, and therefore small-scale techniques have been applied [5,6]. Particularly, nanoindentation has been shown to be suitable, since the size of the tested area and the precision in placing the indenter allow for the determination of the local properties of individual grains [7,8]. In doing so, several researchers have found that high plastic deformation develops directly under the indenter tip [9–11]. Kysar et al. [12] performed an extensive study of the density and distribution of dislocations induced by nanoindentation in nickel single crystals and found that the highest slip activity takes place directly at

the Indenter Penetration Zone (IPZ), i.e., the plastic zone directly ahead of the indenter. These results were also confirmed by simulation studies conducted by Reuber et al. [13].

Following these ideas, an extensive program comprised of different nanoindentation experiments was developed by the authors in order to deform metastable steel samples in a controlled way. Thus, the dynamic deformation was examined by means of cyclic nanoindentation, concluding that metastable stainless steels present an inelastic nature of the unloading/reloading response which is mainly related to the ratcheting effect [14]. The influence of testing mode on the fatigue behavior was also studied, and the results showed that nanoindentation under loading control mode could be compared to conventional low-cycle fatigue tests, whereas the experiments performed under displacement control mode may be associated with high-cycle fatigue tests [15]. Additionally, the dependence of nanoindentation hardness on the crystallographic orientation of austenitic grains was analyzed [8]. Furthermore, the deformation mechanisms induced under both monotonic and cyclic nanoindentation conditions were studied by 3D-Focused Ion Beam (FIB)/Scanning Ion Microscopy (SIM) tomography, confirming that phase transformation from austenite to α'- and ε-martensite are the most relevant mechanisms [16]. Even micropillars were in situ monotonically compressed using a flat punch, and yield stress values were higher than those obtained from the micropillar compression of other austenitic steel grades [6]. This fact was attributed to the presence of transformation-induced martensitic phase in the grain boundaries.

Within this frame, the particular topic described in the present paper, i.e., the plasticity propagation across grain boundaries and its effect on martensitic-induced formation, is relevant in order to complete the assessment of the deformation behavior of metastable austenitic steels. The role of grain boundaries in slip transfer is a topic of recurring interest that has been investigated by Bieler et al. working with Ti and Ta [17], by Scherreriau and Pippan for Cu, Ni, and Fe [18], by Lebensohn and Tomé for Zr alloys [19], and by Di Martino et al. for ferritic steels [20], among others. However, in the particular case of metastable steels, the question becomes more complex due to the subsequent interaction with the martensitic transformation. Therefore, cyclic nanoindentation tests were carried out in order to induce localized deformation on individual austenitic grains, and TEM and Electron Back-Scattered Diffraction (EBSD) were the characterization techniques employed.

2. Materials and Methods

The austenitic stainless steel grade studied was an AISI 301LN (equivalent to EN 1.4318), provided by Outokumpu Stainless Steel (Tornio, Finland) in the form of 1.5-mm-thick sheets. It was delivered in the annealed condition with a fully austenitic microstructure with an average grain size of 12 ± 2 μm and chemical composition as given in Table 1.

Table 1. Chemical composition in wt. %, obtained by microprobe for nitrogen and by energy-dispersive X-ray spectroscopy (EDS) for the other elements.

C	Si	Mn	Cr	Ni	Mo	N	Fe
0.02	0.5	1.3	18.6	6.4	0.1	0.07	balance

For the microstructural and nanomechanical characterization, it was necessary to prepare the surface of interest via mechanical polishing. The different polishing steps were: 30, 6, 3, and 1 μm, in order to slightly reduce the work hardening produced during this polishing process, as phase transformation can be induced due to the metastable nature of the steel. After that, a layer of approximately 100 μm was removed by electrochemical polishing with a solution of 8% perchloric acid.

Prior to the nanoindentation tests, the regions of interest were observed via EBSD in order to access the local crystallographic orientation, as well as to detect the possible presence of martensite remaining after the electropolishing process. A Field Emission Scanning Electron Microscope (FESEM) JEOL7001F (Tokyo, Japan), equipped with an Orientation Imaging Microscopy (OIM) system from

Nordlys (Oxford Instruments, Bucks, England), was employed. EBSD measurements were performed with a constant scanning step of 100 nm at an acceleration voltage of 20 kV.

Nanoindentation tests were performed with a diamond Berkovich indenter, of which the tip radius was approximately 170 nm, in an ultra-nano-hardness tester from CSM Instruments (Neuchâtel, Switzerland). These experiments were carried out under displacement control mode, at a maximum indentation depth (h_{max}) of 250 nm, with a constant loading/unloading rate of 15 mN/min. Tests up to 50 cycles were performed in constant contact with the sample. The complete test sequence was: (i) full loading, (ii) a holding sequence of 10 s in order to stabilize the deformation induced during the process, (iii) unloading up to a minimum load of 0.1 mN, and (iv) reloading. Steps (ii) to (iv) were repeated until the last cycle when the sample was completely unloaded after the last holding sequence.

After nanoindentation testing, TEM lamellae with a size of 5 µm × 5 µm × 500 nm were cut out from the samples by Focused Ion Beam (FIB) using a dual beam workstation Zeiss Neon 40 (Oberkochen, Germany). These lamellae corresponded to cross-sections extracted directly below the center of the desired nanoindentations, i.e., they were cross-sections of the residual nanoimprints. They were lifted out and welded to a copper TEM grid by a micromanipulator, and thinned to electron transparency (<100 nm). During this milling, ion beam energy was kept low in order to avoid eventual phase transformation or damage, which might arise from the interaction with the Ga^+ beam [21,22]. Thus, an initial beam current of 900 pA was chosen for the lift out process, and it was gradually reduced during subsequent polishing steps to 10 pA. The amorphous layer on the surface, eventually caused by the FIB, was removed by plasma cleaning. Following this, the lamellae were introduced into a Philips CM200 (Philips-FEI, Hillsboro, OR, USA), which works at 200 kV, to obtain Bright Field (BF) and Dark Field (DF) images, as well as Selected Area Electron Diffraction (SAED) patterns, from the deformed regions of interest.

3. Results and Discussion

This section is divided into two parts. First, the microstructure of the investigated steel is described by means of EBSD observations. Then, the substructure induced by nanoindentation is characterized by TEM analysis.

3.1. Microstructure Characterization

Figure 1 shows an EBSD map before indentation testing. It can be observed that the initial microstructure is completely austenitic, composed of randomly distributed equiaxial grains with abundant annealing twins.
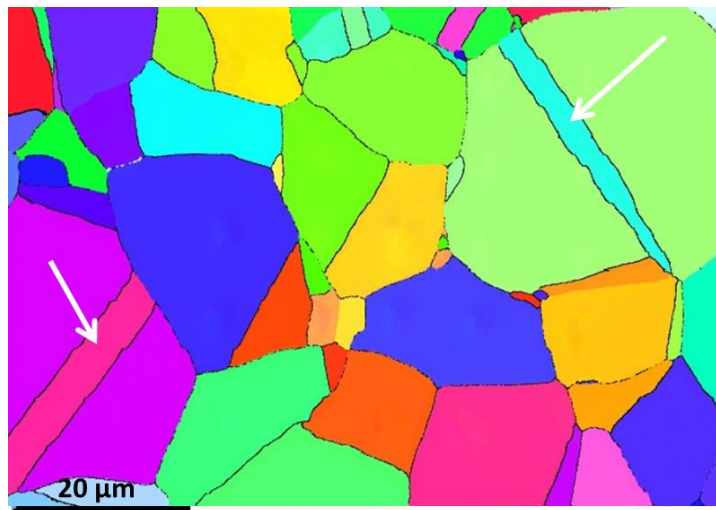
Figure 1. Electron Back-Scattered Diffraction (EBSD) map of a sample before nanoindentation testing. White arrows indicate annealing twins.

After the nanoindentation experiments, neither the formation of twins nor martensitic phase transformation were discerned by EBSD. However, at a closer view, the dark color in the Band Contrast (BC) image indicates the presence of strain accumulation at the immediate surroundings of the indents, as highlighted in Figure 2a. Due to the ductile nature of the steel, the indentation process displaces the material around the residual imprint, known as the pile-up effect. Lattice rotation due to strain accommodation is a phenomenon frequently observed after indentation loading, which has its origin in the generation of Geometrically Necessary Dislocations (GNDs) under the indenter tip, as explained by Dahlberg et al. [23].
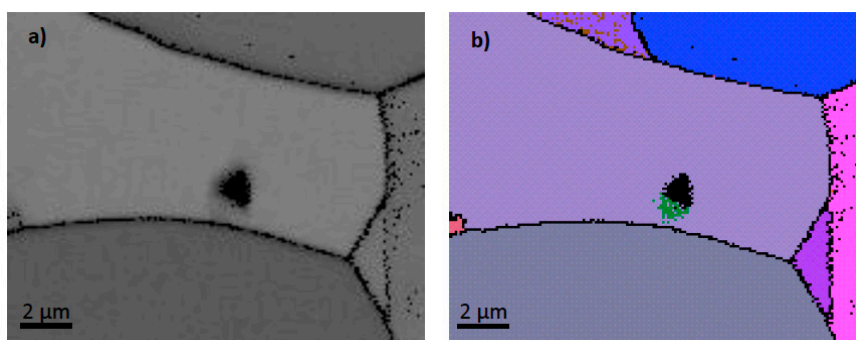

Figure 2. Close view of a nanoindentation imprint. (**a**) EBSD Band Contrast map showing modified contrast around the nanoimprint; (**b**) all-Euler EBSD map exhibiting lattice rotation at one edge of the indent.

3.2. Substructure Characterization

Figure 3 shows different TEM images of the substructure generated after 50 nanoindentation cycles in a <111> oriented grain. The grain boundary (indicated by the red dashed line) is located parallel to the surface, approximately 4 μm beneath it.
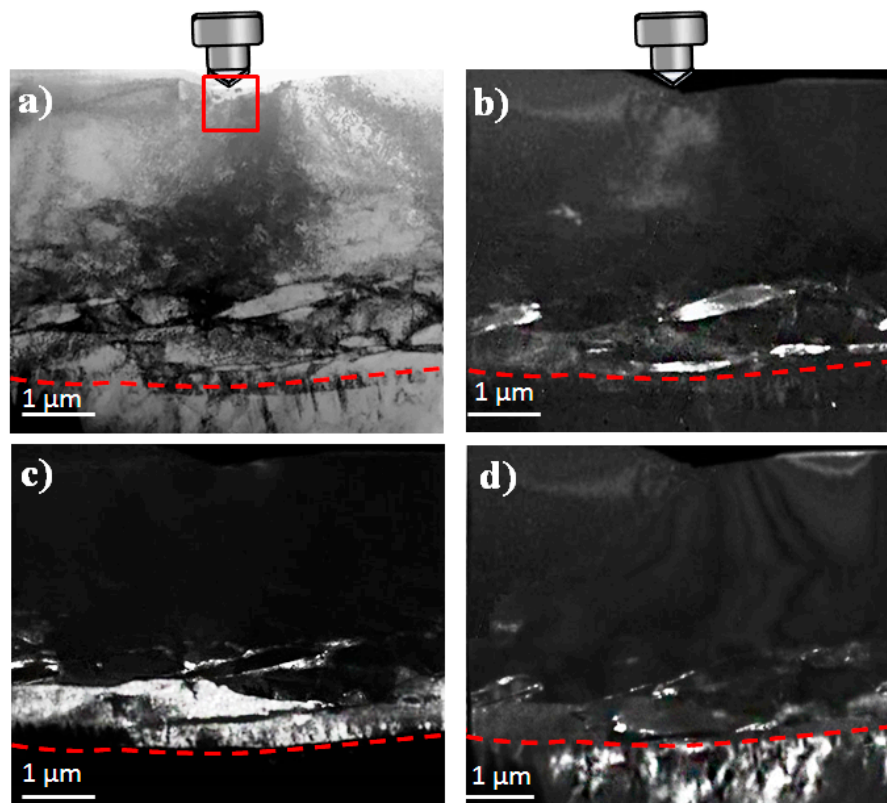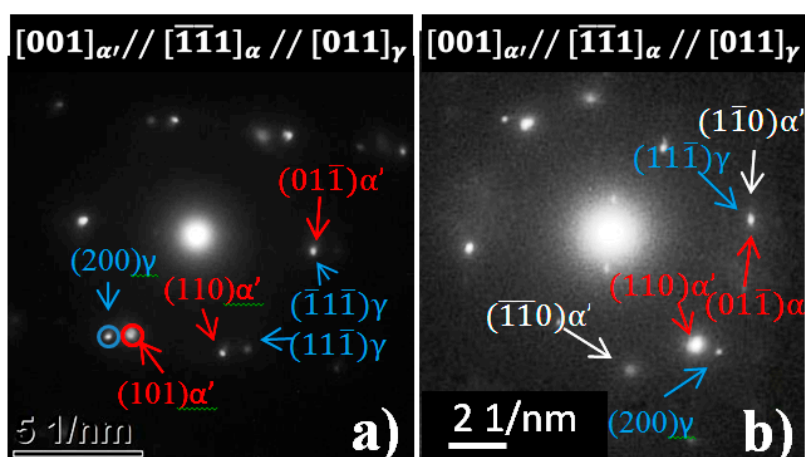
Figure 3. TEM images of the cross-section of a nanoimprint in a <111> oriented grain. (**a**) Bright Field (BF)-TEM image; (**b**) corresponding Dark Field (DF)-TEM image illuminating shear bands; (**c**) DF-TEM image revealing martensite laths; (**d**) DF-TEM image of the austenitic phase at the other side of the grain boundary.

The presence of a thick bundle of shear bands on the (111) plane, parallel to the grain boundary and the surface, is displayed in Figure 3a,b. As revealed by the DF images presented in Figure 3c,d, the shear bands are interwoven with martensitic lamellae. In the case of single indentations, similar deformation features were not observed at grain boundaries located at comparable distances [16].

The plastic zone radius (R_p) corresponding to a nanoimprint is assumed to range between seven to 10 times the maximum indentation depth, as reported by Oliver and Pharr [9]. In the present case, h_max was 250 nm; hence, R_p should be less than 2.5 μm. As the grain boundary was 4 μm below the indentation location, it may be postulated that each indentation cycle generates new dislocations that pile up at the grain boundary, resulting in an increase of the effective size of the plastic zone. When the cumulative strain due to repeated nanoindentations surpasses a threshold value, dislocations can be emitted through the grain boundary into the adjacent grain [24]. Accordingly, Figure 3d shows the deformation features in the neighboring grain due to plasticity transmission across the grain boundary.

Therefore, it can be concluded that strain accumulation due to dislocations pile-up at the grain boundary reached a critical value for shear band formation on planes adjacent to the grain boundary, as well as for α'-martensitic transformation within those bands [25]. This assumption is supported by the fact that the martensitic phase has a Kurdjumov-Sachs relationship [26] to the shear bands. Accordingly, diffraction patterns in Figure 4 show the following orientation relationships: $(111)\gamma \parallel (011)\alpha'$ and $[01\bar{1}]\gamma \parallel [11\bar{1}]\alpha'$, which indicates that the martensitic phase evolved from austenite.

Figure 4. Diffraction patterns corresponding to TEM images of Figure 3. (**a**) Corresponding to Figure 3c; (**b**) corresponding to Figure 3d.

To elucidate those complex diffraction patterns, where spots from three different phases are present, Figure 5 gives a simulated indexed pattern corresponding to Figure 4b. In this pattern, the indentation direction is indicated.

Figure 5. Simulated diffraction pattern corresponding to Figure 4b.

Figure 6 shows a magnified view of the grain boundary zone where a string of particles perpendicular to that boundary can be seen. The corresponding diffraction patterns given in Figure 4; Figure 5 reveal their martensitic nature. More precisely, two martensitic systems can be distinguished: one is oriented in Kurdjumov-Sachs (K-S) relationship with the surrounding austenite matrix, while the other has its [001] zone axis parallel to the austenitic [011] axis, i.e., in a Nishiyam-Wassermann (N-W) orientation relationship (OR) [27].
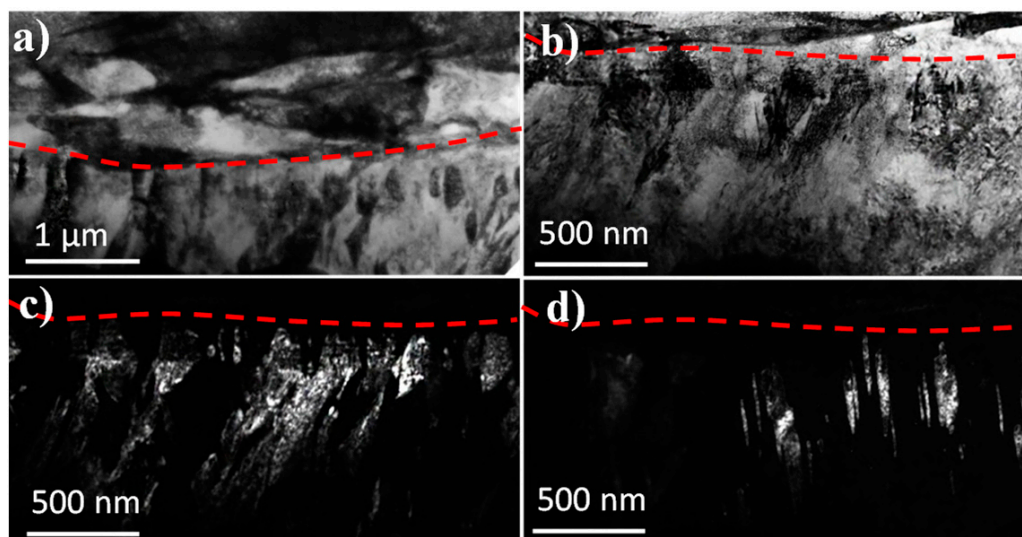
Figure 6. TEM view of the grain boundary region from Figure 3. (**a**) General BF view; (**b**) magnification of the far side of the grain boundary; (**c**) corresponding DF image of [1$\bar{1}$1] oriented martensite; (**d**) DF image illuminating [001] oriented martensite. The approximate position of the grain boundary is marked by dotted red lines.

Martensite in a K-S orientation with austenite grows in the direction of the shear bands observed in Figure 6c, whereas N-W-oriented martensite seems to be in a more incipient development state, exhibiting thin and short needles (Figure 6c,d). From these observations, it is reasonable to postulate that K-S-type martensite nucleated from shear bands, as observed before, while N-W martensite possibly emerged from the grain boundary-shear band intersection, which is also a common martensite formation site in stainless steels [28].

K-S and N-W ORs are regularly observed simultaneously in austenite-martensite transformations in steels, while several factors, such as chemical composition, the prevalence of certain types of dislocations, or thermomechanical history, are decisive in establishing the final predominant OR [29–31]. Moreover, martensite morphology is linked to the OR type. Thus, K-S is known to be preferential for lath martensite, as observed in this study, while N-W is reported for lenticular martensite. Other authors [32] found that in metastable stainless steels, the OR changes from K-S to N-W with the process of deformation. This fact is in agreement with the present observations since α' nucleation at the grain boundary was detected only after slip transfer, e.g., it occurred later than nucleation within intersections of shear bands and subsequent lath formation.

4. Conclusions

The present work has demonstrated that cyclic nanoindentation is a suitable tool to induce strain accumulation, allowing the investigation of the deformation mechanisms with high spatial selectivity and precision. Specifically, the plastic deformation behavior of austenitic grains in commercial metastable steel was analyzed, and the corresponding substructural arrangements produced by indentation testing were studied. Cyclic nanoindentation led to a gradual accumulation and propagation of plasticity, therefore slip transfer into adjacent grains and subsequent martensite transformation was observed.

References

1. Taheri, S.; Hauet, A.; Taleb, L.; Kpodekon, C. Micro–macro investigations about the fatigue behavior of pre-hardened 304L steel. *Int. J. Plast.* **2011**, *27*, 1981–2004. [CrossRef]
2. Santacreu, P.-O.; Glez, J.C.; Roulet, N.; Fröhlich, T.; Grosbety, Y. Austenitic Stainless Steels for Automotive Structural Parts. *SAE Trans.* **2006**, *115*, 805–810.
3. Talonen, J.; Hänninen, H. Formation of shear bands and strain-induced martensite during plastic deformation of metastable austenitic stainless steels. *Acta Mater.* **2007**, *55*, 6108–6118. [CrossRef]
4. Tavares, S.M.; Pardal, J.M.; Gomes, M.J.; Abreu, H.F.G.; Silva, M.R. Deformation induced martensitic transformation in a 201 modified austenitic stainless steel. *Mater. Charact.* **2009**, *60*, 907–911. [CrossRef]
5. Misra, R.D.K.; Zhang, Z.; Jia, Z.; Venkat Surya, P.K.C.; Somani, M.C.; Karjalainen, L.P. Nanomechanical insights into the deformation behavior of austenitic alloys with different stacking fault energies and austenitic stability. *Mater. Sci. Eng. A* **2011**, *528*, 6958–6963. [CrossRef]
6. Roa, J.J.; Wheeler, J.M.; Trifonov, T.; Michler, J.; Fargas, G.; Mateo, A.; Jiménez-Piqué, E. Deformation of polycrystalline TRIP stainless steel micropillars. *Mater. Sci. Eng. A* **2015**, *647*, 51–57. [CrossRef]
7. Ahn, T.-H.; Oh, C.-S.; Kim, D.H.; Oh, K.H.; Bei, H.; George, E.P.; Han, H.N. Investigation of strain-induced martensitic transformation in metastable austenite using nanoindentation. *Scr. Mater.* **2010**, *63*, 540–543. [CrossRef]
8. Roa, J.J.; Fargas, G.; Mateo, A.; Jiménez-Piqué, E. An improved technique for determining hardness and elastic modulus using load and displacement sensing indentation experiments. *J. Mater. Res.* **1992**, *7*, 1564–1583.
9. Oliver, W.C.; Pharr, G.M. On the relationship between plastic zone radius and maximum depth during nanoindentation. *Surf. Coatings Technol.* **2006**, *201*, 4289–4293.
10. Yang, B.; Vehoff, H. Dependence of nanohardness upon indentation size and grain size—A local examination of the interaction between dislocations and grain boundaries. *Acta Mater.* **2007**, *55*, 849–856. [CrossRef]
11. Zaafarani, N.; Raabe, D.; Roters, F.; Zaefferer, S. On the origin of deformation-induced rotation patterns below nanoindents. *Acta Mater.* **2008**, *56*, 31–42. [CrossRef]
12. Kysar, J.W.; Saito, Y.; Oztop, M.S.; Lee, D.; Huh, W.T. Experimental lower bounds on geometrically necessary dislocation density. *Int. J. Plast.* **2010**, *26*, 1097–1123. [CrossRef]
13. Reuber, C.; Eisenlohr, P.; Roters, F.; Raabe, D. Dislocation density distribution around an indent in single-crystalline nickel: Comparing nonlocal crystal plasticity finite-element predictions with experiments. *Acta Mater.* **2014**, *71*, 333–348. [CrossRef]
14. Roa, J.J.; Sapezanskaia, I.; Fargas, G.; Kouitat, R.; Redjaïmia, A.; Mateo, A. Dynamic Deformation of Metastable Austenitic Stainless Steels at the Nanometric Length Scale. *Metall. Mater. Trans. A* **2018**, *49*, 6034–6039. [CrossRef]
15. Roa, J.J.; Sapezanskaia, I.; Fargas, G.; Kouitat, R.; Redjaïmia, A.; Mateo, A. Influence of testing mode on the fatigue behavior of <111> austenitic grain at the nanometric length scale for TRIP steels. *Mat. Sci. Eng. A* **2018**, *713*, 287–293. [CrossRef]
16. Sapezanskaia, I.; Roa, J.J.; Fargas, G.; Turon-Viñas, M.; Trifonov, T.; Kouitat Njiwab, R.; Redjaïmia, A.; Mateo, A. Deformation mechanisms induced by nanoindentation tests on a metastable austenitic stainless steel: A FIB/SIM investigation. *Mater. Charact.* **2017**, *131*, 253–260. [CrossRef]
17. Bieler, T.R.; Eisenlohr, P.; Zhang, C.; Phukan, H.J.; Crimp, M.A. Grain boundaries and interfaces in slip transfer. *Curr. Opin. Solid State Mater. Sci.* **2014**, *18*, 212–226. [CrossRef]
18. Scheriau, S.; Pippan, R. Influence of grain size on orientation changes during plastic deformation. *Mater. Sci. Eng. A* **2008**, *49*, 48–52. [CrossRef]

19. Lebensohn, R.A.; Tomé, C.N. A self-consistent anisotropic approach for the simulation of plastic deformation and texture development of polycrystals: application to zirconium alloys. *Acta Metall. Mater.* **1993**, *41*, 2611–2624. [CrossRef]

20. Di Martino, S.F.; Riddle, N.B.; Faulkner, R.G. Controlling the ductile to brittle transition in Fe-9% Cr ODS steels. *J. Nuclear Mat.* **2013**, *442*, S124–S132. [CrossRef]

21. Knipling, K.E.; Rowenhorst, D.J.; Fonda, R.W.; Spanos, G. Effects of focused ion beam milling on austenite stability in ferrous alloys. *Mater. Charact.* **2010**, *61*, 1–6. [CrossRef]

22. Basa, A.; Thaulow, C.; Barnoush, A. Chemically induced phase transformation in austenite by focused ion beam. *Metall. Mater. Trans. A* **2014**, *45*, 1189–1198. [CrossRef]

23. Dahlberg, C.F.O.; Saito, Y.; Öztop, M.S.; Kysar, J.W. Geometrically necessary dislocation density measurements associated with different angles of indentations. *Int. J. Plast.* **2014**, *54*, 81–95. [CrossRef]

24. Zhang, L.; Ohmura, T.; Shibata, A.; Tsuzaki, K. Characterization of local deformation behavior of Fe–Ni lenticular martensite by nanoindentation. *Mater. Sci. Eng. A* **2010**, *527*, 1869–1874. [CrossRef]

25. Das, A. Dislocation configurations through austenite grain misorientations. *Int. J. Fatigue* **2015**, *70*, 473–479. [CrossRef]

26. Kurdjumov, G.; Sachs, G.Z. Über den Mechanismus der Stahlhärtung. *Z. Phys.* **1930**, *64*, 325–343. [CrossRef]

27. Nishiyama, Z. *Martensitic Transformation*; Fine, M.E., Meshii, M., Waymann, C.M., Eds.; Academic Press: New York, NY, USA, 1978; pp. 480–488.

28. Sabooni, S.; Karimzadeh, F.; Enayati, M.H.; Ngan, H.W. The role of martensitic transformation on bimodal grain structure in ultrafine grained AISI 304L stainless steel. *Mater. Sci. Eng. A* **2015**, *636*, 221–230. [CrossRef]

29. Sato, H.; Zaefferer, S.A. A study on the formation mechanisms of butterfly-type martensite in Fe–30% Ni alloy using EBSD-based orientation microscopy. *Acta Mater.* **2009**, *57*, 1931–1946. [CrossRef]

30. Mine, Y.; Hirashita, K.; Matsuda, M.; Takashima, K. Martensite Formation in Hydrogen-Containing Metastable Austenitic Stainless Steel during Micro-Tension Testing. *Metall. Mater. Trans. A* **2011**, *42*, 3567–3574. [CrossRef]

31. Durlu, T.N. Effects of high austenitizing temperature and austenite deformation on formation of martensite in Fe-Ni-C alloys. *J. Mater. Sci.* **2001**, *36*, 5665–5671. [CrossRef]

32. Yang, H.Y.; Li, J.; Yang, P. The Change of Orientation Relationships between Austenite and α'-Martensite during Deformation in High Manganese TRIP Steel. *Acta Metall. Sin.* **2015**, *28*, 289–294. [CrossRef]